C. R. Geoscience 349 (2017) 151–158

Contents lists available at ScienceDirect

Comptes Rendus Geoscience

www.sciencedirect.com

External Geophysics, Climate

Extent and dynamic evolution of the lost land *aquaterra* since the Last Glacial Maximum

Giorgio Spada *, Gaia Galassi

Dipartimento di Scienze Pure e Applicate (DiSPeA), Università degli Studi di Urbino "Carlo Bo", Via Santa Chiara, 27, 61029 Urbino, Italy

ARTICLE INFO

Article history:
Received 29 June 2017
Accepted after revision 30 June 2017
Available online 23 August 2017

Handled by Philippe Cardin

Keywords:
Paleogeography
Sea-level change
Glacial Isostatic Adjustment

ABSTRACT

We study the evolution of a recently recognised global geographical feature, named *aquaterra*, enclosing those lands that in previous glacial cycles have been repeatedly exposed and flooded. So far, the geography of *aquaterra* has been studied as a first approximation neglecting the isostatic effects and assuming globally uniform *(i.e.* eustatic) sea-level variations. Focussing on the last deglaciation and considering both global and regional aspects, we show that isostatic effects related with mantle dynamics have indeed played a significant role in the evolution of *aquaterra.* Our analysis is based upon paleogeographic reconstructions in the framework of well-established Glacial Isostatic Adjustment theories.

1. Introduction

Dobson (1999) has proposed the recognition of a vast geographical Earth feature – named *aquaterra* – encompassing the lands that have been inundated and exposed during the last 120,000 years in consequence of the waxing and waning of the continental ice sheets. The study of the extent and chronology of *aquaterra* impacts various disciplines of Earth sciences and has also a number of cultural aspects. In particular, knowledge of the detailed evolution of *aquaterra* could shed light on the human history and on the occupation of landmasses in the past (Flemming, 1985), also providing clues on the pathways of diffusion of material culture (Cavalli-Sforza et al., 1993). Recently, Dobson (2014) has refined the description of *aquaterra.* Furthermore, he has also outlined possible strategies for the exploration of *aquaterra*, which would demand a major collaboration between geographers and oceanographers for its exploration.

Before a systematic exploration of *aquaterra* may become possible, global models of Glacial Isostatic Adjustment (GIA, see Spada, 2017, for a review) can be used to constrain its evolution in space and time. Since the seminal work of Peltier (1994), methods for the reconstruction of the ice age paleotopography have become available, based on the solution of the so-called "Sea Level Equation" (SLE) first introduced by Farrell and Clark (1976). The SLE, which describes the time evolution of sea level in response to the melting of the late-Pleistocene ice sheets, can be solved to predict the changing shape of the shorelines, employing suitable high-resolution numerical methods (see Spada and Stocchi, 2007; Spada et al., 2012). In GIA models, the history of sea-level change is determined by taking the variations of the equipotential geoid surface into account and reconstructing the paleotopography iteratively. Earth rotation effects are also accounted for. For these reasons, GIA models are "gravitationally" and "topographically self-consistent" (Peltier, 1994). Isostatic effects are of interest in the present context, since Dobson (2014), as a first approximation, did not take them into account. Thus, so far, the spatial and temporal extent of *aquaterra* has been defined with the

* Corresponding author.
E-mail address: giorgio.spada@gmail.com (G. Spada).

http://dx.doi.org/10.1016/j.crte.2017.06.004

implicit assumption of eustatic (*i.e.* spatially uniform) sea-level variations.

In this note, following the hint of Dobson (2014), we aim at refining the description of *aquaterra* by means of up-to-date GIA modelling. In particular, we shall consider the role of isostasy on the submergence of *aquaterra* since the Last Glacial Maximum (LGM, ~21,000 years ago). During this period, major cultural innovations (see Fig. 3 in Dobson, 2014) and human dispersal occurred (Flemming, 1985; Lahr and Foley, 2004). Furthermore, after LGM existing GIA models define the history of the ice sheets to a sufficient level of detail. By a global analysis and some regional examples, we shall show that dynamic (*i.e.* non-eustatic) processes associated with isostatic deformation, mantle rheology, Earth rotational fluctuations and time variations of topography have affected significantly the extent and evolution of *aquaterra*.

2. Methods

We follow the GIA theory illustrated by Mitrovica and Milne (2003), which generalises the original formulation of the SLE due to Farrell and Clark (1976). The SLE is obtained by imposing mass conservation within the system composed by the Solid Earth, the oceans and the ice sheets, keeping at the same time the sea surface equipotential. The resulting sea-level variations are not uniform across the oceans because of the effects of gravity and deformation, which are delayed as a consequence of the viscoelastic response of the mantle (*e.g.*, Spada, 2017). In the generalised formulation, the SLE accounts for the horizontal migration of shorelines, for the presence of marine-based ice (distinguishing between grounded and floating conditions) and for the effects of rotational feedbacks on sea-level change (Milne and Mitrovica, 1998). The SLE is solved numerically by an improved version of program SELEN (Spada and Stocchi, 2007; Spada et al., 2012), employing an icosahedron-based equal-area grid (Tegmark, 1996) with a spacing of ~20 km, sufficient to describe the isostatic effects on the global distribution of *aquaterra* in detail. The length of the integration time step is 0.5 kyr.

In this study, following the suggestion by Dobson (2014), we account for glacial isostasy adopting the global deglaciation chronology ICE-5G(VM2) of Peltier (2004) for the continental ice complexes. It assumes isostatic equilibrium before the LGM, and no deglaciation during the last 4 kyr. ICE-5G(VM2) is constrained to fit a global set of relative sea-level (RSL) data and represents a refinement of previous ICE-X models developed by W. R. Peltier (see, *e.g.*, Peltier, 2004, and references therein). The ice thicknesses of continental ice sheets at the LGM and at present time according to ICE-5G(VM2) are shown in Fig. 1. In this work, we adopt a volume-average of the original multilayered viscosity profile VM2 (Peltier, 2004), with a viscosity of 2.7, 0.5, and 0.5×10^{21} Pa·s in the lower mantle, transition zone and shallow upper mantle, respectively. The thickness of the elastic lithosphere is 90 km. It is worth noting that GIA models are affected by some uncertainty, associated with limited knowledge about the melting history of the ice sheets and the rheology of the Earth. As a consequence, it should be taken into consideration that different GIA models can provide slightly different predictions for the history of sea-level change, which will also affect the features and evolution of *acquaterra*.

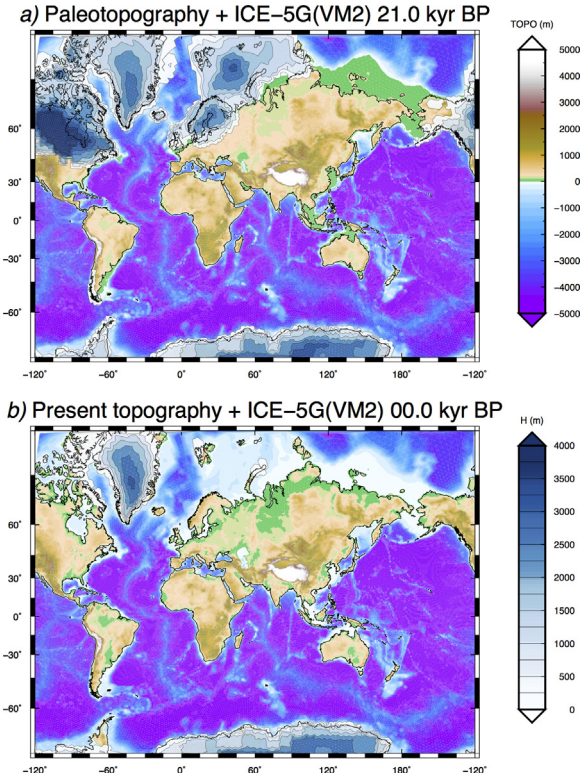

Fig. 1. Paleo-topography al the LGM, reconstructed solving the SLE (a). The present-day topography, corresponding to ETOPO1, is shown in (b). The global ice thickness distribution according to the GIA model ICE-5G(VM2) is also shown.

Following Mitrovica and Milne (2003), paleobathymetry is reconstructed by performing two nested iterations of the SLE. In the internal iteration, the SLE is solved for a given *a priori* distribution of bathymetry; in the external one, the bathymetry is updated be means of the pattern of relative sea-level change obtained in the internal iteration. This procedure is performed adopting the "bedrock version" of the one arc-minute resolution ETOPO1 global relief (Amante and Eakins, 2009) as the present-day condition. The Earth's topographies at the LGM and at present time are shown in Fig. 1.

3. Results

We first consider the evolution of *aquaterra* from a global viewpoint; then we show results obtained for a few regional case studies.

3.1. A global view

A first guess of the global distribution of *aquaterra* since the LGM is shown in Fig. 2a, where blue pixels mark a grid cells belonging to *aquaterra*. To obtain this map, which is

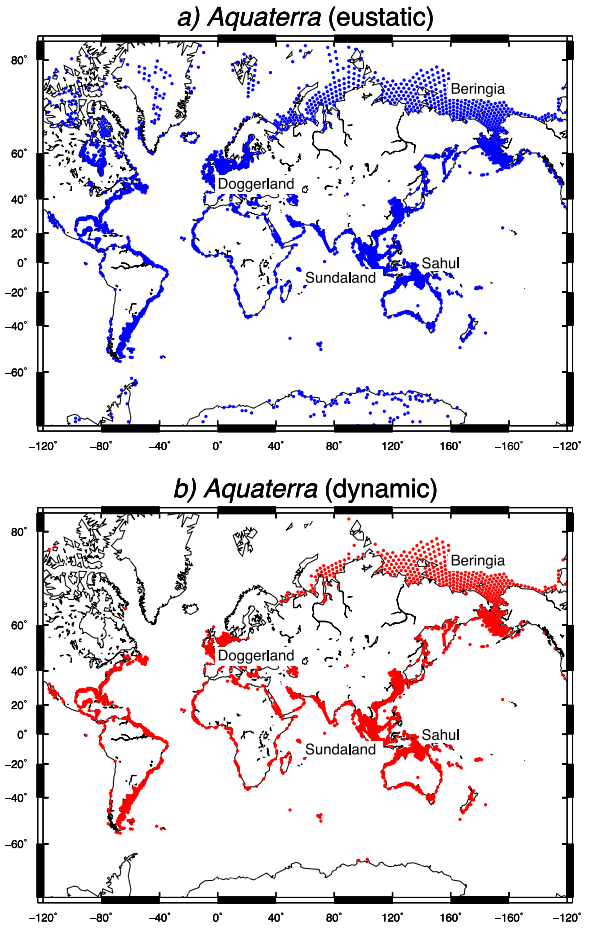

Fig. 2. The spatial distribution of *aquaterra* according to the eustatic (a) and to the dynamic model (b). Major recognised land bridges, *i.e.* Beringia, Doggerland, Sundaland and Sahul, are also shown. Note that the Mercator projection exaggerates the polar region areas

broadly in agreement with that in Dobson (2014), we have subtracted 127.3 m of water from the globally gridded ETOPO1 distribution, corresponding to the total equivalent sea-level rise since the LGM according to ice model ICE-5G(VM2). Hence, what we have obtained in this way is independent of the history and of the actual geographical distribution of past ice sheets, being determined by the present bathymetry and on the total volume of ice melt since the LGM. Such an approximation is equivalent to assume a spatially uniform *(i.e.* eustatic) sea-level rise across the ocean basins. Since eustasy implies the assumption of a rigid Earth and of negligible gravitational interactions between the solid Earth, the ice sheets and the oceans (see, *e.g.*, Spada, 2017), the *aquaterra* map in Fig. 2a has a static rather that a dynamic character. According to the eustatic approximation, the area of *aquaterra* amounts to 22.5×10^6 km^2, *i.e.* 4.4% of the area of the Earth's surface. Note the limited development of *aquaterra* below 45° S, due to the relatively narrow and unusually deep Antarctic continental shelf (Padman et al., 2010). Some basic statistics about the spatial distribution of *aquaterra* are shown in Table 1. A prevalence of *aquaterra* in the northern

Table 1
Statistics of the spatial distribution of *aquaterra* across three latitudinal sectors, according to the dynamic and to the eustatic definition.

Sector	*Aquaterra* (dynamic) area (km^2)	%	*Aquaterra* (eustatic) area (km^2)	%	Range of latitude (°)
North	4,808,790	28	8,331,195	37	$\varphi \geq +45°$
Centre	11,873,805	69	12,176,880	54	$-45° \leq \varphi \leq +45°$
South	491,655	3	1,946,415	9	$\varphi \leq -45°$
Total	17,174,250	100	22,454,490	100	

hemisphere is also confirmed for the past 120,000 years (Zong, 2015).

It is interesting to compare the static *aquaterra* distribution in Fig. 2a with that obtained when the GIA problem is solved consistently; this is shown in Fig. 2b by red pixels. Based on our paleotopographic reconstruction (two snapshots are shown in Fig. 1), these are the pixels that are currently submerged, but that have been emerged and ice-free at least during one time step (*i.e.* for 500 years) since the LGM. According to this dynamic definition (others are possible, indeed), *aquaterra* mostly occupies the continental shelf and, at mid and low latitudes, it contours most of the world's shorelines, in qualitative agreement with Dobson (2014) and with Fig. 2a. However, the introduction of isostatic effects has significant quantitative consequences. For example, the area of *aquaterra* is $\sim 17.2 \times 10^6$ km^2, which approximately corresponds to 3.4% of the area of the whole Earth's surface. This is a sizeable reduction (by $\sim 25\%$) with respect to the eustatic distribution of *aquaterra.* At high latitudes, the *aquaterra* distribution is quite complex and shows a major development in correspondence of the East Siberian Sea and Beringia. When the GIA problem is solved consistently, *aquaterra* disappears from part of the Hudson Bay, from the Canadian Arctic Archipelago, and from the Baltic Sea (compare with Fig. 2a). Some of the pixels belonging to these regions are now below sea level, but since the LGM they have never been emerged (nor ice-free) in consequence of the isostatic depression caused by the former ice sheets. It is worth noting that the distribution of *aquaterra* across Doggerland, located in the periphery of the previous Würm ice sheet, is affected by isostasy. The same occurs in the Baltic Sea region. The extension of *aquaterra* in Beringia appears to be less affected, since this region has been ice-free since the LGM and isostatic disequilibrium has been important. However, a more quantitative account of the dynamic effects acting across these regions requires the study of the sea-level curves from specific locations, which will be done in Section 3.2 below.

The blue curve in Fig. 3 shows the area of *aquaterra* since the LGM, obtained by the dynamic model. The plot provides insight into the time evolution of *aquaterra*, which can be broadly divided into three major phases, each with a duration of ~ 7000 years. During the early and the late phases, the area has remained close to stationary, while during the central period the *aquaterra* has been subject to a major reduction until its substantial disappearance. In the central phase, however, the evolution of *aquaterra* has been quite complex, and characterised by

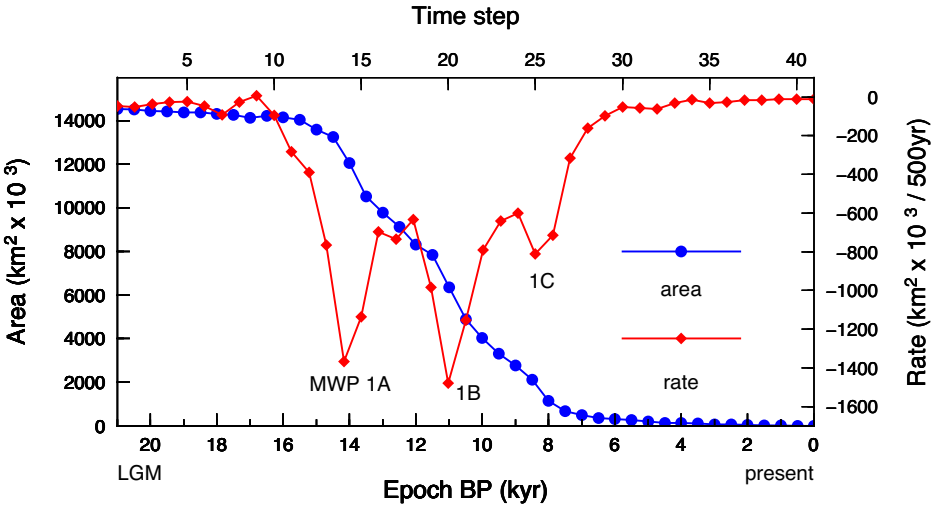

Fig. 3. History of the exposed area of *aquaterra* (blue) and of its rate of change (red) from the LGM to present, according to the dynamic *aquaterra* model. The times of occurrence of the three meltwater pulses MWP-1A, 1B and 1C are also shown.

intermittent variations in consequence of the pulses of ice-sheet meltwater that occurred within this time frame (Fairbanks, 1989; Fairbanks et al., 1992; Gornitz, 2013; Stanford et al., 2011). These can be better visualised by computing the time-derivative of the history of the *aquaterra* area (red curve), which is indeed marked by three minima corresponding to periods of enhanced loss of area, corresponding to Melt Water Pulses MWP-1A, 1B, and 1C (Blanchon, 2011; Gornitz, 2013). Although MWP-1A (between 14.3 and 12.8 ka BP) is of a multi-centennial to millennial nature, MWP-1B can be more appropriately described by a broad multi-millennial peak between 11.5 and 8.8 ka BP (Stanford et al., 2011), which partly overlaps with MWP-1C. The origin of meltwater pulses has been discussed in a number of studies (*e.g.*, Clark et al., 1996, 2002; Gomez et al., 2015; Peltier, 2004) and is still a matter of debate (Abdul et al., 2016; Blanchon, 2011; Liu et al., 2016). In the ice model that we have employed here, *i.e.* ICE-5G(VM2), MWP-1A fully originates from the northern hemisphere, while for MWP-1B there is a substantial contribution also from Antarctica (Peltier, 1998, 2004). Remarkably, these two pulses produce comparable effects on the rate of disappearance of *aquaterra*, at ~ 14 and ~ 11 kyr BP, respectively.

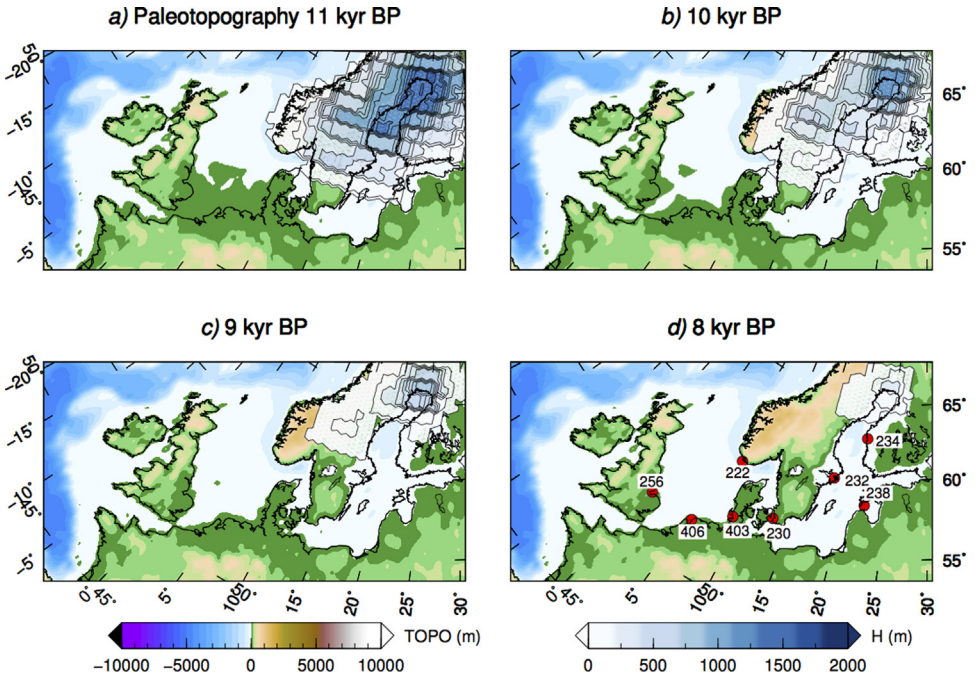

Fig. 4. Paleotopography of northern Europe and ice thickness evolution according to model ICE-5G(VM2) in the time window between 11 and 8 kyr BP.

3.2. A few regional case studies

Fig. 4 shows the paleotopography across the western North Sea and the Baltic Sea between 11 and 8 kyr BP, according to our GIA modelling. The area currently located between southern Britain and Jutland was the site, since the LGM, of the large alluvial plain known as Doggerland (Coles, 2000; Ward et al., 2006), which bridged Britain with continental Europe. Its maximum emergence occurred between 15 and 12 ky BP (Lambeck, 1995), when it was open to periglacial vegetation and was occupied by human settlements (Ward et al., 2006). Fig. 4 shows the formation of Doggerland Island, the last remain of Doggerland (Coles, 2000; Shennan et al., 2000), before its final submergence ca. 8200 years ago, possibly as a consequence of the tsunami caused by the Storegga Slide (Weninger et al., 2008). We note in Fig. 4 that the evolution of the coastlines of Doggerland has been particularly rapid between 11 and 10 kyr BP (frames a and b), as a consequence of MWP-1B (see Fig. 3).

To the east of Doggerland, the evolution of the Baltic Sea during the last deglaciation has been characterised by a complex development of the shorelines, controlled by deglaciation dynamics, isostatic rebound and erosion (Bjorck, 1995). According to the paleotopographic reconstruction of Fig. 4, during the time period between 11 and 8 kyr BP, a major reduction of the Würm ice sheet extension occurred, accompanied by a northward migration of $\sim$ 500 km of its meridional margin. This has caused a differential isostatic adjustment (Bjorck, 1995), which has enhanced the complex evolution of the geographical features in the region (Kostecki, 2014). Fig. 4 shows the late stage of Ancylus Lake, a fresh water lake, just before the transition to the Littorina Sea (Bendixen et al., 2017). According to our GIA model predictions, the Littorina Sea transgression occurred between $\sim$ 9 and $\sim$ 8 kyr BP across the Great Belt (see frames c and d), in substantial agreement with the reconstruction of Kostecki (2014).

Fig. 5a and b show relative sea-level (RSL) curves for some locations in northern Europe, in the Baltic Sea and in Britain (the locations are marked by red dots in Fig. 4a). The sites are listed in the Tushingham and Peltier (1992, 1993) database, from which RSL data are available. Here, however, we are not concerned with a comparison between model predictions and RSL observations. Rather, we are aimed at assessing the amount of isostatic disequilibrium across the region by a comparison of RSL predictions with the eustatic sea-level (ESL) curve, shown by a dashed line. Due to the strong uplift caused by the melting of the former Würm ice sheet that covered the area at the LGM, RSL curves from the Baltic Sea show a sea-level fall, opposite to the eustatic sea-level increase. The kink at $\sim$ 14 kyr BP marks the occurrence of MWP-1A, which has caused an accelerated RSL fall in this region. The large isostatic rebound in the Baltic Sea strongly affects the evolution of paleogeography in the area, which confirms the importance of a non-eustatic approach in the definition of *aquaterra*. In the periphery of the former Doggerland (id. 256, 403 and 406), RSL curves are clearly non-monotonic (Peltier, 1998) and strongly deviate from ESL during the first phase of deglaciation, until MWP-1A. Later on, the RSL curves indicate that isostasy has generally reduced the amount of sea-level rise that we would expect from eustasy, leaving however unchanged the general monotonous trend.

Fig. 6 shows the late evolution stages of the land bridge that once connected Siberia to Alaska, named Beringia after Hulten (1937). As shown in Fig. 2, this land mass constitutes a sizeable portion of *aquaterra*. The evolution of Beringia, which had profound implications on human dispersal pattern over North America (see *e.g.*, Clark et al., 2014; Gore, 1997; Hoffecker et al., 2016), has been detailed in a number of studies (see, *e.g.*, Elias et al., 1996; Hopkins et al., 1967; McManus et al., 1983). Of particular interest is the timing of the postglacial flooding of Beringia, which has been long discussed. Based on a well-dated core from the

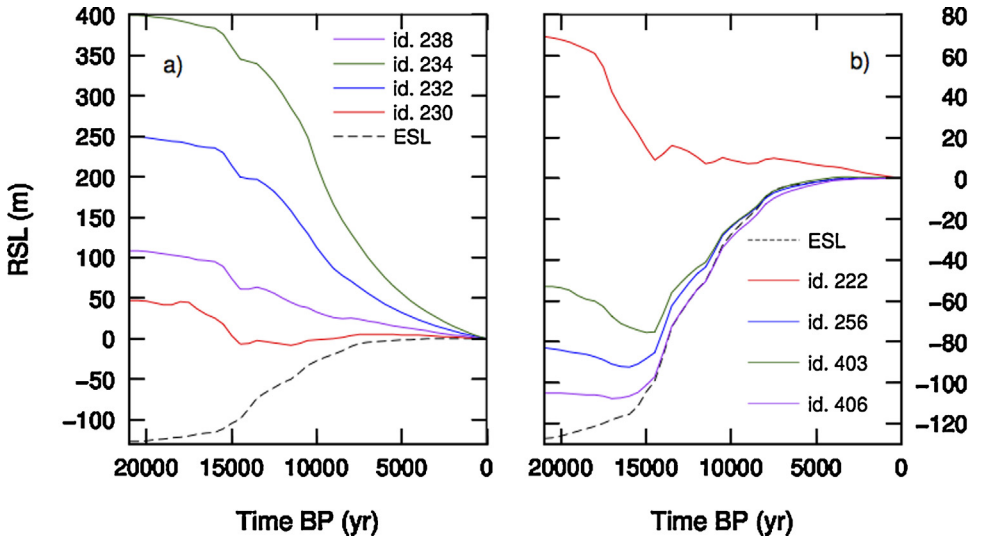

Fig. 5. RSL curves at the eight locations shown by red dots in Fig. 4d. ESL (dashed) denotes the eustatic curve.

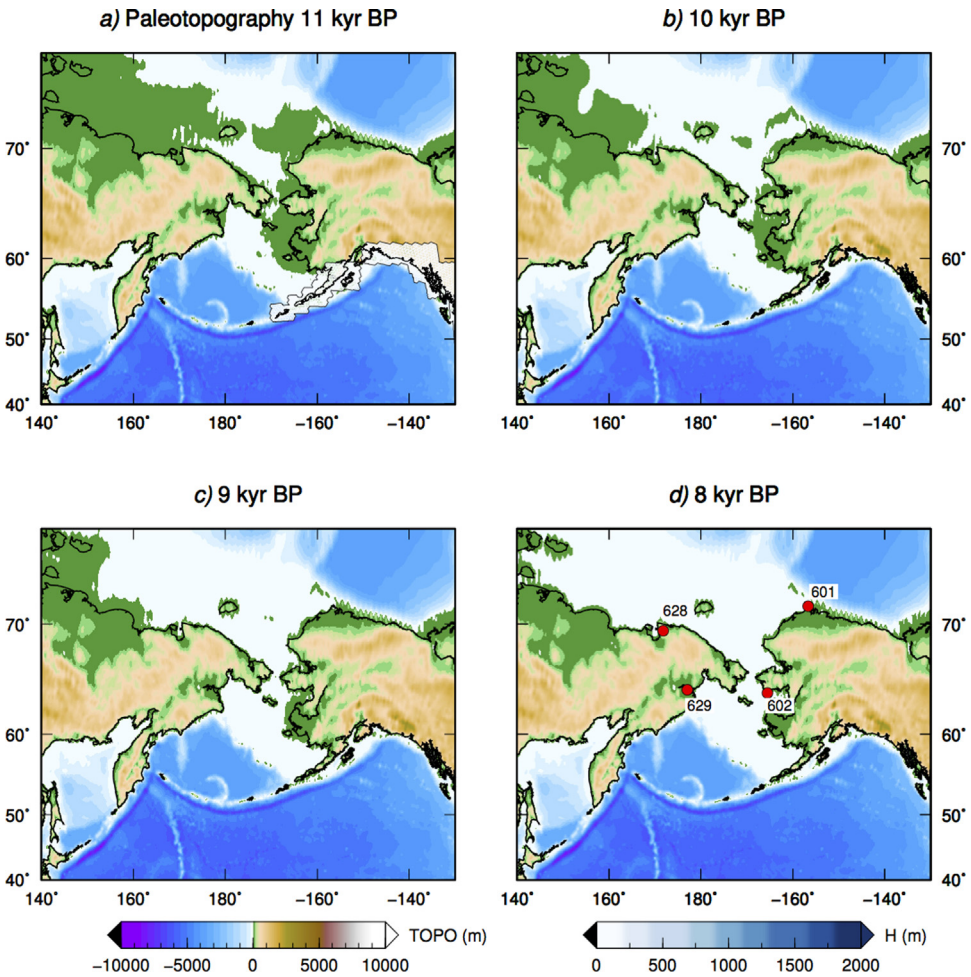

Fig. 6. Paleotopography of the Bering Strait between 11 and 8 kyr BP, according to the GIA model computations. The flooding of Beringia occurs between 11 and 10 kyr BP.

Herald Canyon, very recently Jakobsson et al. (2017) have suggested that the transition from a near-shore environment to an open marine setting occurred ∼ 11 kyr BP, at the time of MWP-1B (see Fig. 3). This fairly agrees with our reconstruction of Fig. 6, showing that the transition occurred between 11 and 10 kyr BP, accompanied by a major disappearance of landmasses from the Arctic Sea. The timing of the flooding event appears to be sensitive to the GIA model employed, however. For example, in Peltier (1998), who adopted the ICE-4G model (Peltier, 1994), the closure of the Beringia land bridge was predicted to have occurred ∼ 9 kyr ago. Computations based on the recent ICE-6G(VM5a) model (Peltier et al., 2015) now support the findings of Jakobsson et al. (2017). To our knowledge, a systematic study of the sensitivity of the time of flooding to the GIA model parameters has not been attempted so far. Using field data, this could potentially provide new constraints on the deglaciation chronology and possibly on mantle rheology.

In Fig. 7, we show some RSL curves from Alaska (id. 601 and 602 in Fig. 6) and from Eurasia (628 and 629), with coordinates from the Tushingham and Peltier database.

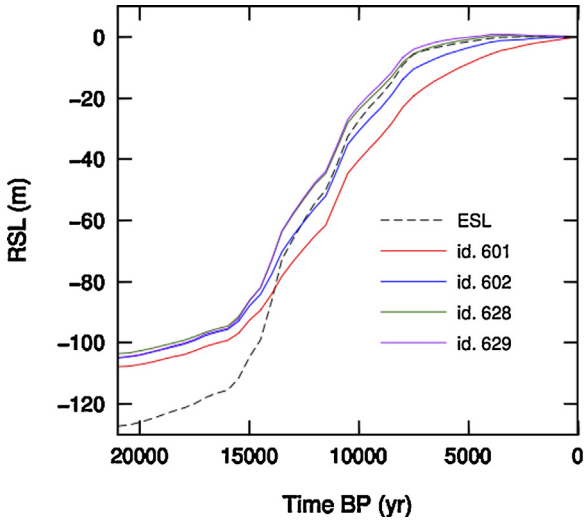

Fig. 7. RSL curves from four locations facing the Bering Strait, marked by red dots in Fig. 6. ESL (dashed) is the sea-level curve according to the eustatic theory.

Differently from northern Europe (see Fig. 5) in this area the RSL curves are clearly monotonous. Deviations from the ESL curve are large before MWP-1A (∼ 14 kyr BP), but they remain significant also afterwards, especially for sites 601 and 602, located relatively close to the formerly Laurentian ice sheet and thus potentially more affected by isostatic disequilibrium. In particular, site 602 is facing the Bering Strait, adjacent to the place where flooding occurred according to our modelling. This indicates that non-eustatic effects have indeed played a role in the timing of the disappearance of the Beringia bridge (and consequently in the evolution of *aquaterra*), which supports the argument of Jakobsson et al. (2017) about the importance of isostasy in the region.

4. Conclusions

Using a GIA model, we have studied the spatial and temporal evolution of *aquaterra* since the LGM. The SLE has been solved assuming the global deglaciation model ICE-5G(VM2) of Peltier (2004) and taking into consideration all the physical processes that account for non-eustatic sea-level changes. Our conclusions can be summarised as follows:

i) Dynamic effects play an important role in the evolution of *aquaterra*, particularly above 45°N. When they are taken into account, the extension of exposed *aquaterra* is decreased by ∼ 25% with respect to the eustatic case. This contributes to a better description of the deepest boundaries of *aquaterra, i.e.* the maximum extent of where humans could have directly influenced the landscape
ii) The history of the size of *aquaterra* is characterised, between ∼ 14 and ∼ 7 kyr BP by a major reduction, punctuated by abrupt decreases at the time of meltwater pulses MWP-1A, 1B and 1 C. Before MWP-1A and since ∼ 7 kyr BP, changes in the area of *aquaterra* have been minor
iii) As expected, dynamic effects associated with GIA play an important role in the evolution of *aquaterra* in the regions that once were covered by thick ice, like the Baltic Sea region. In the surroundings of Doggerland and across the Bering Strait, they have been less pronounced, but still significant. The timing of the major events like the disappearance of some important *aquaterra* features like Dogger Island and the Bering Strait bridge appears to the tightly related with MWP-1B (∼ 11 kyr BP). The predicted epoch of these episodes, however, is rather sensitive to the choice of the GIA model.

Acknowledgments

This work is dedicated to Claude Froidevaux, with gratitude for having welcomed GS at the Laboratoire de géologie de l'École normale supérieure (Paris) in 1991 and for a number of very stimulating discussions on several occasions. We are indebted to Luce Fleitout and Jerry Dobson for very valuable comments that have considerably improved the manuscript. We thank Giada Salciccia for her help with the paleogeographic reconstructions. Work funded by research grants of the Department of Pure and Applied Sciences (DiSPeA) of the Urbino University (CUP H32I160000000005). We have used data from the NOAA sea-level database http://www1.ncdc.noaa.gov/pub/data/paleo/paleocean/relativeseaJevel/. Program SELEN can be downloaded from https://geodynamics.org/cig/software/selen/or requested to the authors. The figures have been drawn using the Generic Mapping Tools (GMT) of Wessel and Smith (1998).

References

Abdul, N.A., Mortlock, R.A., Wright, J.D., Fairbanks, R.G., 2016. Younger Dryas sea level and meltwater pulse 1B recorded in Barbados reef crest coral *Acropora palmata*. Paleoceanography 31 (2), 330–344.
Amante, C., Eakins, B., 2009. ETOPO1 Arc-minute global relief model: procedures, data source and analysis. Tech. rep 1–19.
Bendixen, C., Jensen, J.B., Boldreel, L.O., Clausen, O.R., Bennike, O., Seidenkrantz, M.S., Nyberg, J., Hübscher, C., 2017. The Holocene Great Belt connection to the southern Kattegat, Scandinavia: Ancylus Lake drainage and Early Littorina Sea transgression. Boreas 46 (1), 53–68.
Bjorck, S., 1995. A review of the history of the Baltic Sea, 13.0–8.0 ka BP. Quat. Int. 27, 19–40.
Blanchon, P., 2011. Meltwater pulses, Encyclopedia of Earth Science Series. Encyclopedia of modern coral reefs: structure, form and process, Encyclopedia of Earth Science Series, Springer, pp. 683–690 [http://unam.academia.edu/PaulBlanchon/Papers]
Cavalli-Sforza, L.L., Menozzi, P., Piazza, A., 1993. Demic expansions and human evolution. Science 259, 639.
Clark, J., Mitrovica, J.X., Alder, J., 2014. Coastal paleogeography of the californiaoregon-washington and bering sea continental shelves during the latest Pleistocene and Holocene: implications for the archaeological record. J. Archaeol. Sci. 52, 12–23.
Clark, P.U., Alley, R.B., Keigwin, L.D., Licciardi, J.M., Johnsen, S.J., Wang, H., 1996. Origin of the first global meltwater pulse following the last glacial maximum. Paleoceanography 11 (5), 563–577.
Clark, P.U., Mitrovica, J., Milne, G., Tamisiea, M., 2002. Sea-level fingerprinting as a direct test for the source of global meltwater pulse IA. Science 295 (5564), 2438–2441.
Coles, B.J., 2000. Doggerland: the cultural dynamics of a shifting coastline. Geol. Soc. London, Spec Publ. 175 (1), 393–401.
Dobson, J., 1999. Explore Aquaterra-Lost Land Beneath the Sea. Geo. World 12, 30–31.
Dobson, J.E., 2014. Aquaterra incognita: Lost land beneath the sea. Geo. Rev. 104 (2), 123–138.
Elias, S.A., Short, S.K., Nelsonif, C.H., Birks, H.H., 1996. Life and times of the Bering land bridge. Nature 382, 4.
Fairbanks, R.G., 1989. A 17,000-year glacio-eustatic sea level record: influence of glacial melting rates on the Younger Dryas event and deep-ocean circulation. Nature 342 (6250), 637–642.
Fairbanks, R.G., Charles, C.D., Wright, J.D., 1992. Origin of global meltwater pulses. In: Radiocarbon after four decades. Springer, 473–500.
Farrell, W., Clark, J., 1976. On postglacial sea-level. Geophys. J. Roy. Astr. S. 46, 647–667.
Flemming, N., 1985. Ice ages and human occupation on the continental shelf. Oceanus 28.1, 18–25.
Gomez, N., Gregoire, L., Mitrovica, J., Payne, A., 2015. Laurentide-Cordilleran Ice Sheet saddle collapse as a contribution to meltwater pulse 1A. Geophys. Res. Lett. 42 (10), 3954–3962.
Gore, R., 1997. The most ancient Americans. Natl Geogr. 192 (4), 92–99.
Gornitz, V., 2013. Rising seas: past, present, future. Columbia University Press.
Hoffecker, J.F., Elias, S.A., O'Rourke, D.H., Scott, G.R., Bigelow, N.H., 2016. Beringia and the global dispersal of modern humans. Evol. Anthropol. 25 (2), 64–78.
Hopkins, D.M., et al., 1967. The Bering land bridge, 3. Stanford University Press.
Hulten, E., 1937. Outline of the history of arctic and boreal biota during the Quaternary period: their evolution during and after the glacial period as indicated by the equiformal progressive areas of present plant species. Bokfourglas aktiebogelat Thule, Stockholm.

Jakobsson, M., Pearce, C., Cronin, T.M., Backman, J., Anderson, L.G., Barrientos, N., Bjourk, G., Coxall, H., de Boer, A., Mayer, L.A., Muorth, C.-M., Nilsson, J., Rattray, J.E., Stranne, C., Semilietov, I., O'Regan, M., 2017. Postglacial flooding of the Beringia Land Bridge dated to 11,000 cal yrs BP based on new geophysical and sediment records. Climate of the Past Discussions. 1–22 [http://www.clim-past-discuss.net/cp-2017-11/]

Kostecki, R., 2014. Stages of the Baltic Sea evolution in the geochemical record and radiocarbon dating of sediment cores from the Arkona Basin. Oceanolog. Hydrobiol. Stud. 43 (3), 237–246.

Lahr, M.M., Foley, R.A., 2004. Demography, dispersal and human evolution in the last glacial period. In: Van Andel, T., Davies, W. (Eds.), Neanderthals and modern humans in the European landscape during the last glaciation: archaeological results of the stage 3 project. McDonald Institute for Archaeological Research, pp. 241–256.

Lambeck, K., 1995. Late Devensian and Holocene shorelines of the British Isles and North Sea from models of glacio-hydro-isostatic rebound. J. Geol. Soc. 152 (3), 437–448.

Liu, J., Milne, G.A., Kopp, R.E., Clark, P.U., Shennan, I., 2016. Sea-level constraints on the amplitude and source distribution of Meltwater Pulse 1A. Nat. Geosci. 9 (2), 130–134.

McManus, D., Creager, J., Echols, R., Holmes, M., 1983. The Holocene transgression on the Arctic flank of Beringia: Chukchi valley to Chukchi estuary to Chukchi Sea. Quaternary Coastlines and Marine Archaeology. Academic Press, London365–388.

Milne, G., Mitrovica, J., 1998. Postglacial sea-level change on a rotating Earth. Geophys. J. Int. 133 (1), 1–19.

Mitrovica, J.X., Milne, G.A., 2003. On postglacial sea level: I. Gen. Theory Geophys. J. Int. 154 (2), 253–267.

Padman, L., Costa, D.P., Bolmer, S.T., Goebel, M.E., Huckstadt, L.A., Jenkins, A., McDonald, B.I., Shoosmith, D.R., 2010. Seals map bathymetry of the antarctic continental shelf. Geophys. Res. Lett. 37 (21.) .

Peltier, W., 1998. Postglacial variations in the level of the sea: implications for climate dynamics and solid-earth geophysics. Rev. Geophys. 36 (4), 603–689.

Peltier, W., 2004. Global glacial isostasy and the surface of the ice-age Earth: the ICE-5G (VM2) model and GRACE. Ann. Rev. Earth Planet. Sci. 32, 111–149.

Peltier, W., Argus, D., Drummond, R., 2015. Space geodesy constrains ice age terminal deglaciation: the global ICE-6G_C (VM5a) model. J. Geophys. Res. 120 (1), 450–487.

Peltier, W.R., 1994. Ice age paleotopography. Science 265 (5169), 195.

Shennan, I., Lambeck, K., Flather, R., Horton, B., McArthur, J., Innes, J., Lloyd, J., Rutherford, M., Wingfield, R., 2000. Modelling western North Sea palaeogeographies and tidal changes during the Holocene. Geol. Soc. London Spec. Publ. 166 (1), 299–319.

Spada, G., 2017. Glacial isostatic adjustment and contemporary sea level rise: an overview. Surv. Geophys. 38 (1), 1–33.

Spada, G., Melini, D., Galassi, G., 2012. Modeling sea level changes and geodetic variations by glacial isostasy: the improved SELEN code. arXiv preprint 1212.5061. .

Spada, G., Stocchi, P., 2007. SELEN: a Fortran 90 program for solving the "Sea Level Equation". Comput. Geosci. 33 (4), 538–562.

Stanford, J.D., Hemingway, R., Rohling, E.J., Challenor, P.G., Medina-Elizalde, M., Lester, A.J., 2011. Sea-level probability for the last deglaciation: a statistical analysis of far-ield records. Glob. Planet. Ch. 79 (3), 193–203.

Tegmark, M., 1996. An icosahedron-based method for pixelizing the celestial sphere. Astrophys. J. 470, L81.

Tushingham, A., Peltier, W., 1992. Validation of the ICE-3G model of Wuerm-Wisconsin deglaciation using a global data base of relative sea level histories. J. Geophys. Res. 97 (B3), 3285–3304.

Tushingham, A., Peltier, W., 1993. Relative Sea Level Database. IGPB PAGES/World Data Center-A for Paleoclimatology Data Contribution Series. Tech. Rep. 93–106.

Ward, I., Larcombe, P., Lillie, M., 2006. The dating of Doggerland – postglacial geochronology of the southern North Sea. Environ. Archaeolog. 11 (2), 207–218.

Weninger, B., Schulting, R., Bradtmöller, M., Clare, L., Collard, M., Edinborough, K., Hilpert, J., Joris, O., Niekus, M., Rohling, E.J., et al., 2008. The catastrophic final flooding of Doggerland by the Storegga Slide tsunami. Doc. Praehistor. 35, 1–24.

Wessel, P., Smith, W.H.F., 1998. New, improved version of Generic Mapping Tools released. Eos T. Am. Geophys. Un. 79 (47), 579.

Zong, C., 2015. Late Pleistocene sea levels and resulting changes in global land distributions. (Ph. D. thesis) University of Kansas, USA.